AGU PUBLICATIONS

JGR

Journal of Geophysical Research: Oceans

RESEARCH ARTICLE

10.1002/2017JC013652

Reconstructing Tropical Pacific Sea Level Variability for the Period 1961–2002 Using a Linear Multimode Model

Richard J. Greatbatch[1,2], **Xiaoting Zhu**[1], **and Martin Claus**[1,2]

[1]Ocean Circulation and Climate Dynamics, GEOMAR Helmholtz Centre for Ocean Research Kiel, Kiel, Germany, [2]Faculty of Mathematics and Natural Sciences, University of Kiel, Kiel, Germany

Key Points:
- A linear, multimode model driven by reanalysis wind stress products has skill at reproducing monthly mean sea level variability as measured by tide gauges in the presatellite era
- A spurious eastward trend in the zonal wind stress in the NCEP/NCAR product leads to a spurious upward trend in model-computed sea level in the eastern Pacific
- The pivot point at the equator was further west during 1993–2014 than earlier due to an upward trend in zonal wind stress variance in the western equatorial Pacific

Correspondence to:
R. J. Greatbatch,
rgreatbatch@geomar.de

Citation:
Greatbatch, R. J., Zhu, X., & Claus, M. (2018). Reconstructing tropical pacific sea level variability for the period 1961–2002 using a linear multimode model. *Journal of Geophysical Research: Oceans*, *123*, 2037–2048. https://doi.org/10.1002/2017JC013652

Received 27 NOV 2017
Accepted 26 FEB 2018
Accepted article online 2 MAR 2018
Published online 15 MAR 2018

Abstract Monthly mean sea level anomalies in the tropical Pacific for the period 1961–2002 are reconstructed using a linear, multimode model driven by monthly mean wind stress anomalies from the NCEP/NCAR and ERA-40 reanalysis products. Overall, the sea level anomalies reconstructed by both wind stress products agree well with the available tide gauge data, although with poor performance at Kanton Island in the western-central equatorial Pacific and reduced amplitude at Christmas Island. The reduced performance is related to model error in locating the pivot point in sea level variability associated with the so-called "tilt" mode. We present evidence that the pivot point was further west during the period 1993–2014 than during the period 1961–2002 and attribute this to a persistent upward trend in the zonal wind stress variance along the equator west of 160° W throughout the period 1961–2014. Experiments driven by the zonal component of the wind stress alone reproduce much of the trend in sea level found in the experiments driven by both components of the wind stress. The experiments show an upward trend in sea level in the eastern tropical Pacific over the period 1961–2002, but with a much stronger upward trend when using the NCEP/NCAR product. We argue that the latter is related to an overly strong eastward trend in zonal wind stress in the eastern-central Pacific that is believed to be a spurious feature of the NCEP/NCAR product.

1. Introduction

In the tropical Pacific, simplified ocean models (e.g., reduced-gravity, shallow water models) driven by estimates of the observed wind stress are able to reproduce sea level fluctuations not only on the interannual time scale (Qiu & Chen, 2012; Zhu et al., 2017) but also on decadal and multidecadal time scales (Qiu & Chen, 2012; Timmermann et al., 2010). However, before the satellite era, the only direct measurements of sea level are from tide gauges, mostly located on islands, resulting in a very sparse spatial coverage compared to that from the satellite altimeter, leading to uncertainty in the variability of sea level in the presatellite era on a range of time scales (Rhein et al., 2013). There are also uncertainties in simulated and projected sea level rise in climate models (Church et al., 2013), not least arising from uncertainties in the initial conditions used for future projections (Bordbar et al., 2015).

Given that a multimode linear model has considerable success at reproducing interannual sea level variability in the tropical Pacific as seen by the satellite altimeter (Zhu et al., 2017), one way to estimate sea level variability in the presatellite era is to run the same model using estimates of the surface wind stress from reanalysis, e.g., the 40 year European Centre for Medium-Range Weather Forecasts (ECMWF) Reanalysis (ERA-40) (Kalnay et al., 1996) and/or the National Center for Environmental Prediction/National Center for Atmospheric Research (NCEP/NCAR) Reanalysis (Uppala et al., 2005). However, these wind stress products are, themselves, subject to error that can, in turn, lead to errors in the simulated sea level variability. The problem is highlighted by a recent study using the Max Planck Institute Earth System Model (Pohlmann et al., 2017). These authors demonstrate that a large artificial trend in NCEP/NCAR-zonal wind stress in the eastern-central tropical Pacific reduces the hindcast prediction skill for sea surface temperature in the tropical Pacific when the NCEP/NCAR product is used as part of the initialization.

The objective of the present study is to reconstruct monthly sea level variability in the equatorial Pacific for the period 1961–2002 using the linear, multimode model of Zhu et al. (2017) driven by monthly mean wind stress fields from the NCEP/NCAR and ERA-40 reanalysis products. The multimodel of Zhu et al. (2017) has its origin in the early work by Busalacchi and O'Brien (1981) and Busalacchi et al. (1983). However, unlike

those early studies that consider only a single baroclinic normal mode, Zhu et al. (2017) consider the first five baroclinic normal modes. They also do not specify a vertical structure for the wind forcing term; rather, the vertical structure is derived by fitting model-computed sea level variability to that seen by satellite data along the equator. Nagura and McPhaden (2010) take a similar approach to modeling the equatorial Indian Ocean but restricting to long, equatorial waves (waves for which the zonal flow is in geostrophic balance along the equator) and using a method based on McCreary (1981) to project the wind forcing onto the different vertical modes. Likewise, Qiu and Chen (2012) have used a nonlinear, $1\frac{1}{2}$ layer model driven by observed wind stress to simulate tropical Pacific sea level variability over the period 1993–2009.

The paper is organized as follows. In section 2, the model setup and data are described. In section 3, we show the reconstructed sea level anomalies obtained using the linear, multimode model and validate the model performance against the available tide gauge and satellite data. We also examine the model-computed trends in sea level and the impact of the trend in the NCEP/NCAR reanalysis noted by Pohlmann et al. (2017) on the modeled sea level. The interannual variability is, not surprisingly, dominated by El Niño-Southern Oscillation (ENSO) events (Becker et al., 2012) and leads us into a discussion of the pivot point in the western-central Pacific that is a manifestation of the "tilt" mode of Clarke (2010) and the associated trends in zonal wind stress variance. Finally, section 4 provides a summary and discussion.

2. Methods

We adopt the linear, multimode model described in Zhu et al. (2017). This model is a linear combination of linear, shallow water models for the first five baroclinic vertical normal modes (see Gill (1982) and McCreary (1981) for a discussion of vertical normal modes). The weighting given to each mode is the same as used in Zhu et al. (2017) and was obtained by running the model using monthly mean wind stress anomalies from ERA-Interim and fitting the simulated sea level anomalies along the equator to those of the satellite altimeter measured sea level anomalies produced by Ssalto/Duacs and distributed by AVISO with support from Cnes (http://www.aviso.altimetry.fr/duacs/; hereafter, this data set is referred to as AVISO). Readers who are interested in the details are referred to Zhu et al. (2017).

In our experiments, except for the wind forcing, the model configuration is the same as in Zhu et al. (2017), including the model domain (12°S–18°N, 112°E–70°W), coastline (300 m isobath), horizontal resolution (0.5°×0.5°), boundary conditions (solid walls at the eastern/western boundaries, sponge layers applied to the momentum equations at the northern/southern boundaries with e-folding scale of 5° in latitude) and a horizontal eddy viscosity of 5,000 $m^2\ s^{-1}$.

Two standard experiments are, respectively, driven by monthly mean wind stress anomalies from the National Center for Environmental Prediction/National Center for Atmospheric Research (NCEP/NCAR hereafter) Reanalysis (Uppala et al., 2005) and the 40 year European Centre for Medium-Range Weather Forecasts (ECMWF) Reanalysis (ERA-40 hereafter) (Kalnay et al., 1996). Both model runs are carried out for the period from the 1 September 1957 to the 1 August 2002 and the analysis period is 1 January 1961 to 1 August 2002 to exclude the model spin-up.

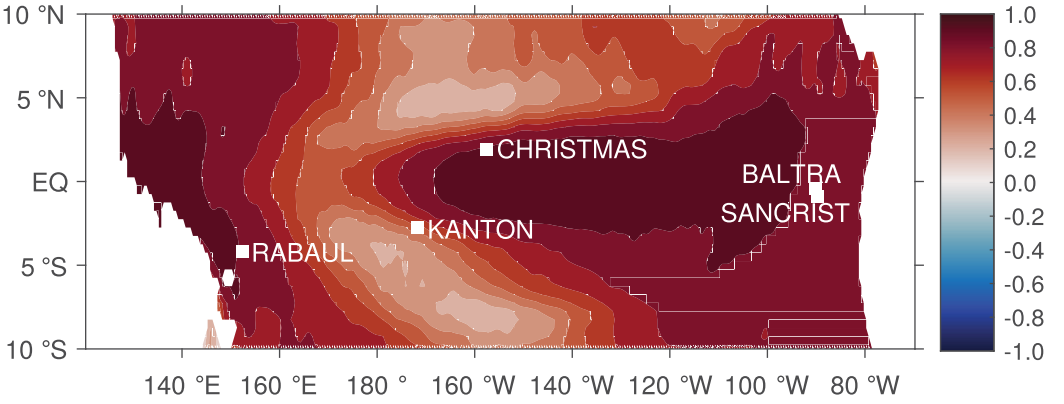

Figure 1. Locations of tide gauge stations (white squares): Rabaul in the western basin, Kanton Island and Christmas Island in the central basin, Baltra Island and Sancrist Island in the eastern basin. The contour shading denotes the correlation between monthly means of AVISO and model-computed sea level for the period 1993–2014 (using the same color scale as in Figure 6a of Zhu et al. (2017) and note that there are no negative correlations in the region shown).

The wind stress anomalies are referenced to the respective monthly mean wind stress climatologies from NCEP/NCAR and ERA-40 for the analysis period 1961–2002. These two standard experiments are called the NCEP/NCAR experiment and the ERA-40 experiment, respectively. In addition, we also conduct two sensitivity experiments forced only by zonal wind stress anomalies from the NCEP/NCAR and ERA-40 data sets; these experiments are called NCEP/NCAR-zonal and ERA-40-zonal, respectively. We also make use of the results from the standard experiment of Zhu et al. (2017) that is driven by monthly mean wind stress anomalies from the ERA-Interim reanalysis (Berrisford et al., 2009). In this experiment, the anomalies are referenced to the period 1993–2014.

To validate the model, we use sea level obtained from the tide gauge stations marked in Figure 1. The data were downloaded from the Permanent Service for Mean Sea Level (Holgate et al., 2013; PSMSL, 2016). We also use the satellite measured sea level anomalies from January 1993 to September 2014 from AVISO at $1/4°$ resolution in latitude and longitude.

3. Results

3.1. The Model Performance

To gain an overview of the model performance, we first show Hovmoeller diagrams of the zonal wind stress and sea level anomalies along the equator from the NCEP/NCAR and ERA-40 experiments (Figure 2). Both

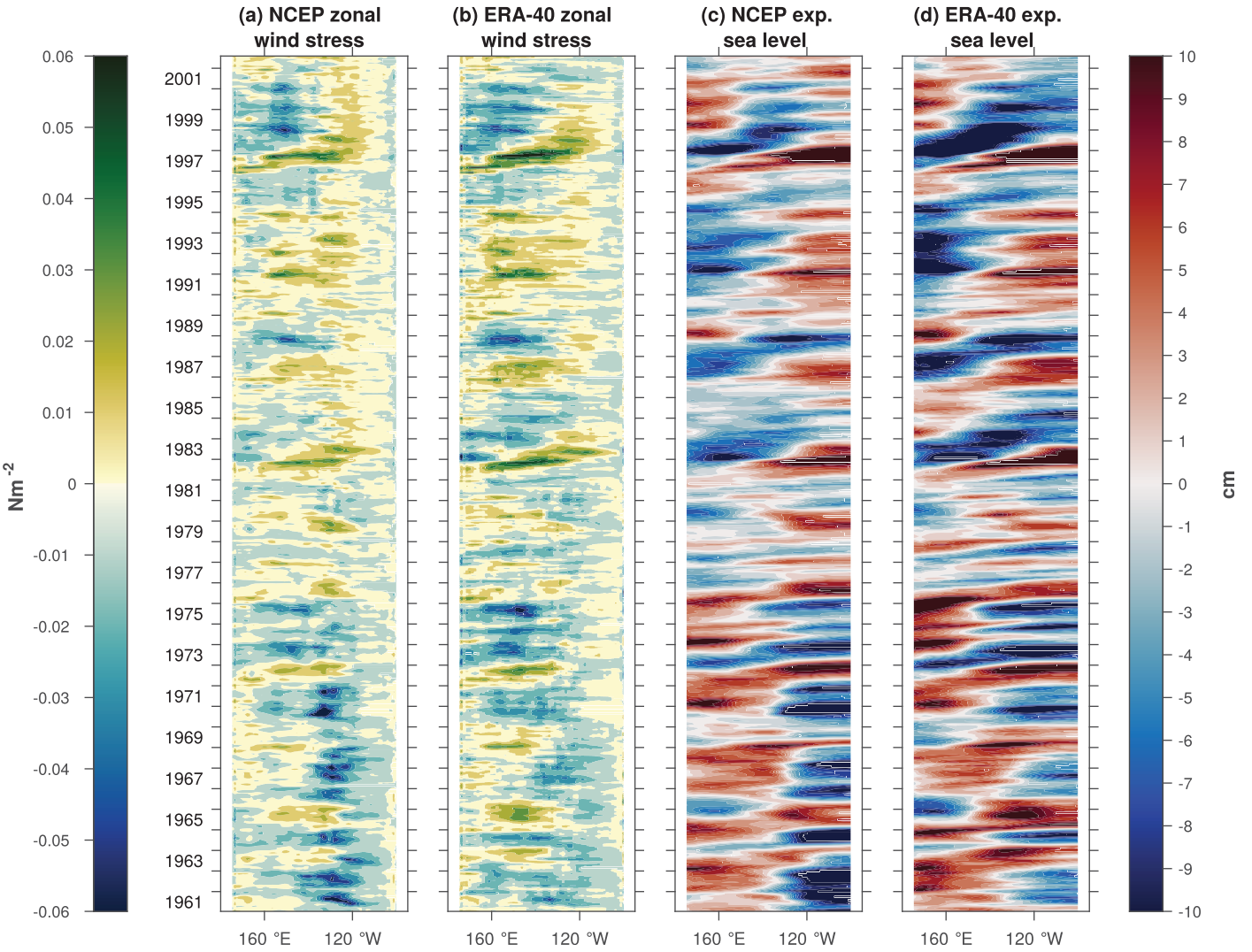

Figure 2. Hovmoeller diagrams along the equator, showing monthly means of zonal wind stress anomalies from (a) the NCEP/NCAR and (b) the ERA-40 products, and model-computed sea level anomalies from (c) the NCEP/NCAR experiment and (d) the ERA-40 experiment.

experiments reproduce the documented El Niño events (e.g., 65/66, 72/73, 82/83, 86/87, and 97/98 El Niños) and La Niña events (e.g., 64/65, 70/71, 84/85, 88/89, and 99/00 La Niñas) (Wang & Fiedler, 2006), where the 86/87 El Niño (Ashok et al., 2007) and the 88/89 La Niña (Capotondi et al., 2015) are examples of Modoki ENSO events. Comparing the two experiments, NCEP/NCAR-zonal wind stress anomalies (Figure 2a) experience a large eastward trend near 120°W during 1961–2002, which is missing from ERA-40 (Figure 2b), as reported by Pohlmann et al. (2017). There is a corresponding positive trend in sea level in the eastern equatorial Pacific basin in the case driven by NCEP/NCAR wind stress anomalies (Figure 2c) that, again, is missing from the ERA-40 experiment (Figure 2d) and which we discuss further in section 3.2. An interesting feature of the results of both experiments is the presence of a "pivot" point near the center of the basin about which the modeled sea level along the equator has a tendency to tip up and down, as in a see-saw. The presence of the pivot point is the manifestation of the "tilt" mode that has been discussed by Clarke (2010). The pivot point was noted by Zhu et al. (2017) in their model experiments and is also found in AVISO, a topic we discuss in more detail in section 3.3.

To evaluate the performance of the models in more detail, Figure 3 compares the sea level anomaly time series from the NCEP/NCAR and ERA-40 experiments with the tide gauge observations at the five tide gauge stations marked in Figure 1 (all data are monthly means). As a check, the tide gauge data are verified against AVISO, i.e., during the satellite era, in Figure 4, from which it is clear that there is good agreement. (Note the suggestion of a problem with the tide gauge at Rabaul between 1995 and 1998 given the offset

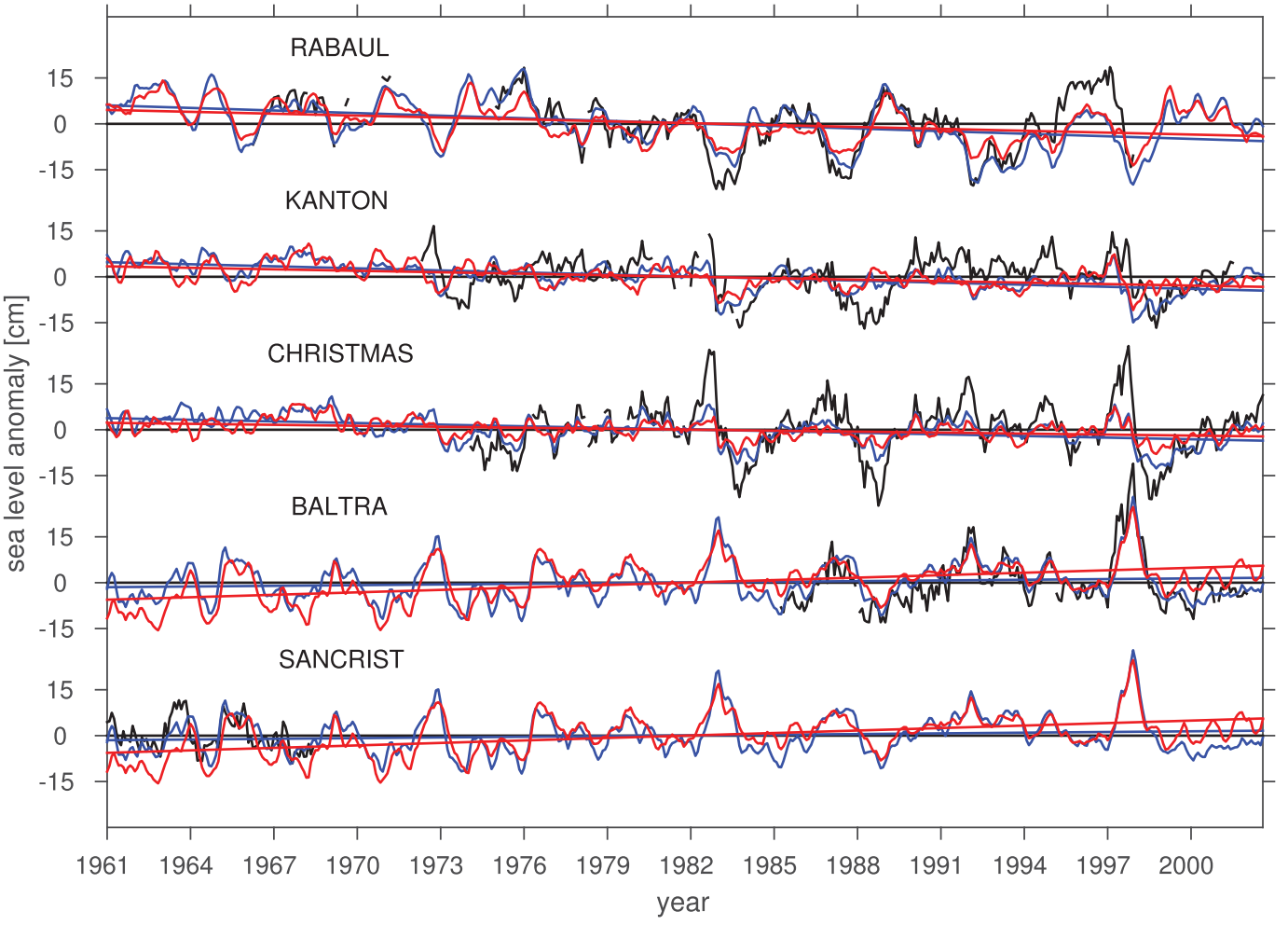

Figure 3. The time evolution of monthly mean sea level anomalies (in cm) from the tide gauge measurements (black lines), the NCEP/NCAR experiment (red lines), and the ERA-40 experiment (blue lines) at the tide gauge locations shown in Figure 1. Trends are shown by corresponding, colored straight lines. Here the labeling on the *x* axis refers to 1 January of each year. Note also that there is only a short time period, from 1961 to 1968, for which data are available from Sancrist.

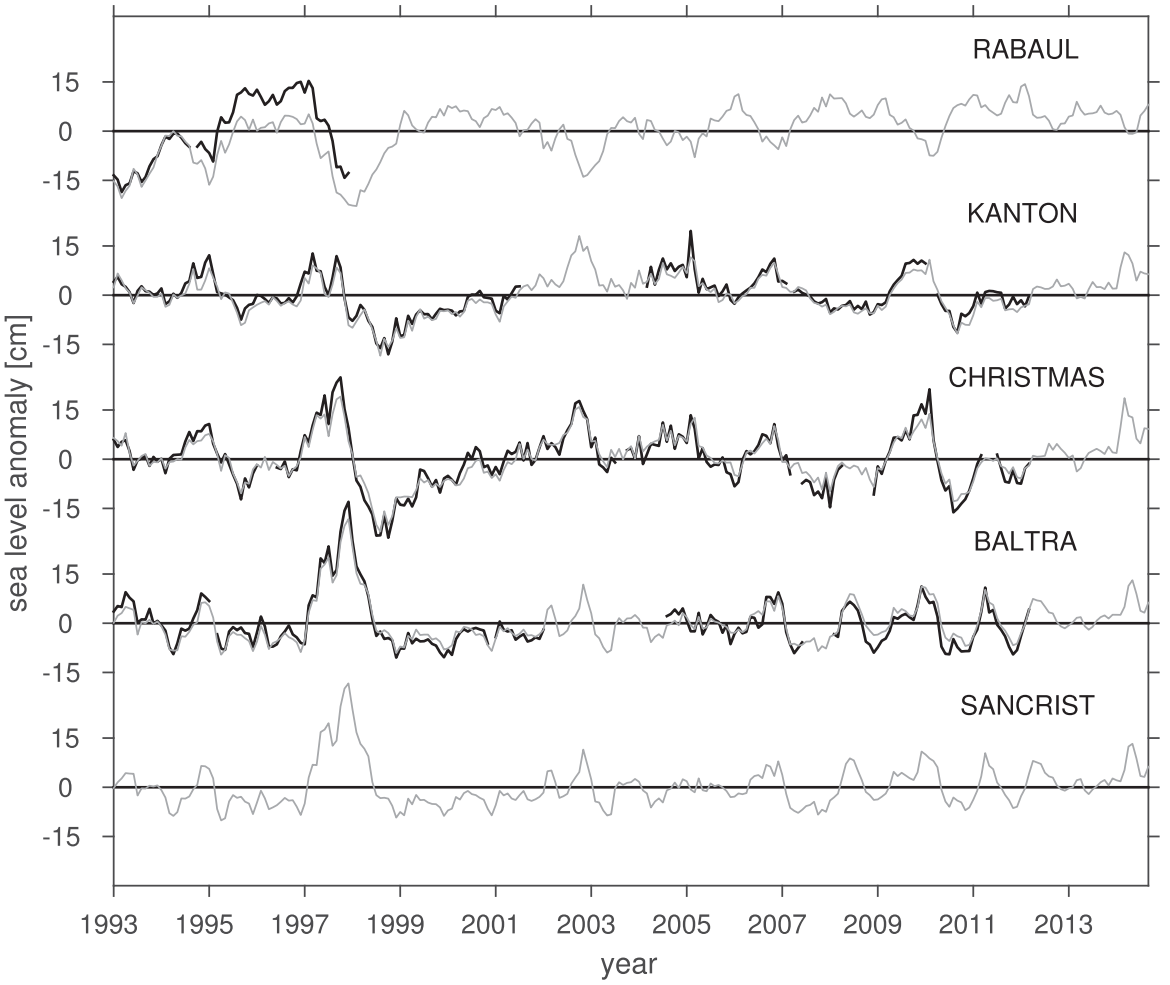

Figure 4. The time evolution of monthly mean sea level anomalies (in cm) from the tide gauge measurements (black) and satellite altimetry measurements (gray) at the tide gauge locations shown in Figure 1. As in Figure 3, the labeling on the *x* axis refers to 1 January of each year. Note also that no tide gauge data are available from Sancrist for the AVISO period.

from AVISO during this period, an offset that is not present before 1995.) Looking at Figure 3, we see that the model has skill at reproducing the interannual sea level variations. To quantify this, we compute the correlations between observed and reconstructed sea level at Rabaul (4.2°S, 152.2°E), Kanton (2.8°S, 171.7°W), Christmas (2.0°N, 157.5°W) and Baltra (0.4°S, 90.3°W) for the time period 1985–1997 for which we have almost continuous tide gauge records (any data gaps are filled by linear interpolation). During this 13 year long period, the correlations at Rabaul, Kanton, Christmas, and Baltra for the NCEP/NCAR (ERA-40) experiments are 0.85 (0.82), 0.09 (0.31), 0.68 (0.87), and 0.84 (0.84), respectively. Based on the method of Ebisuzaki (1997), these correlations are significantly different from zero at the 95% level with the exception of those at Kanton. The drop off in correlation at Kanton is consistent with the spatial pattern of correlation for the period 1993–2014 between AVISO and the model-computed sea level anomalies noted by Zhu et al. (2017) and shown by the color shading in Figure 1. The region of relatively low correlation near Kanton Island is, in turn, related with the misplacement of the pivot point in the model, a topic we return to in section 3.3. At Christmas Island, the model has skill at capturing events, especially in the ERA-40 experiment, but generally underestimates the amplitude, consistent with Figure 5 in Zhu et al. (2017) (in particular, compare their Figures 5a and 5b). Interestingly, the region of reduced correlation near Kanton Island is also the region in which Bunge and Clarke (2014) argue that the relationship between variations in sea surface height and the depth of the 20°C isotherm is obscured by the influence of rainfall. These authors note the importance of zonal advective processes in this region (see also Dewitte et al., 2013), processes that are missing from the

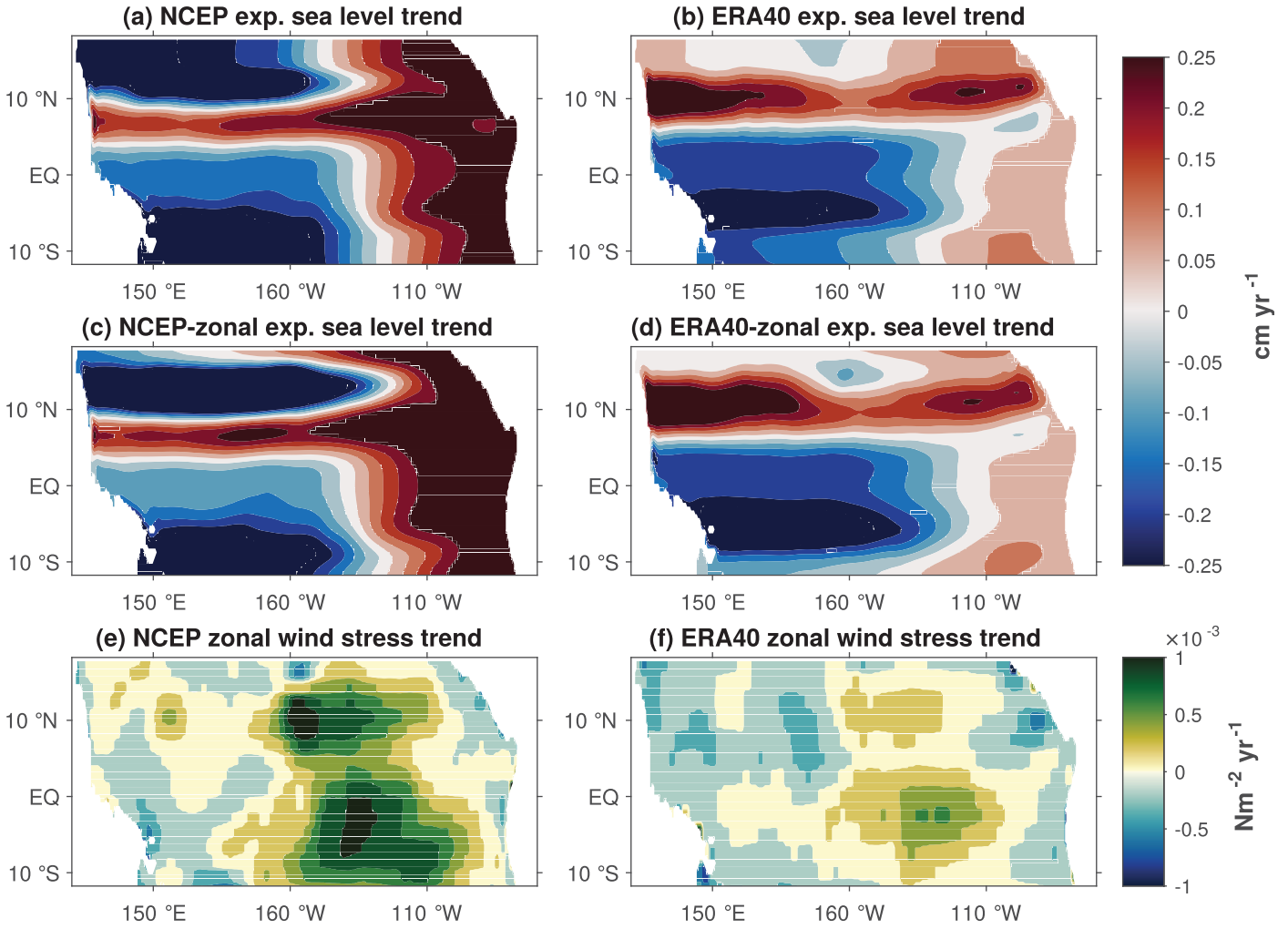

Figure 5. Spatial pattern of the trend in sea level over the period 1961–2002 (in cm yr^{-1}) in (a) the NCEP/NCAR experiment, (b) the ERA-40 experiment, (c) the NCEP/NCAR-zonal experiment, and (d) the ERA-40-zonal experiment, as well as the corresponding trend in the zonal wind stress anomalies (in N m^{-2} yr^{-1}) from (e) the NCEP/NCAR and (f) the ERA-40 products.

multimode model and which Zhu et al. (2017) argue contribute to the reduced performance of their model in this region.

3.2. The Trends in Model-Computed Sea Level

In addition to the interannual variability, Figure 3 also shows the trend in the model time series at the locations of the tide gauges. It is notable that the NCEP/NCAR experiments shows an upward trend at Sancrist and Baltra in the eastern equatorial Pacific that is much stronger than that found in the ERA-40 experiment. This difference in the trend between the two experiments in the eastern equatorial Pacific is clear when looking at Figures 5a and 5b. To determine the origin of the trend, we use the experiments driven by only the zonal wind stress: the NCEP/NCAR-zonal experiment and the ERA-40-zonal experiment. The spatial distribution of the sea level trend in these experiments is shown in Figures 5c and 5d and is very similar to that in Figures 5a and 5b. It follows that the zonal wind stress primarily determines the model-computed sea level trend in the tropical Pacific. Furthermore, it is clear that the large positive trend in sea level in the eastern tropical Pacific in the NCEP/NCAR experiment is associated with the large eastward trend in zonal wind stress in the NCEP/NCAR product (Figure 5e) that, in turn, has been attributed as spurious by Pohlmann et al. (2017). It follows that the large upward trend in sea level in the NCEP/NCAR experiment is almost certainly spurious and that the weaker upward trend in the ERA-40 experiment is more reliable. Indeed, both NCEP/NCAR and ERA-40-zonal wind stress anomalies exhibit an eastward trend, corresponding

to a weakening of the Walker circulation associated with the 1976–1977 climate shift (Trenberth et al., 1998), but this is much stronger in the NCEP/NCAR case. Qiu and Chen (2012), by considering the later period 1993–2009, noted the opposite trend in tropical Pacific sea level to that noted here, in both AVISO data and in a nonlinear 1½ layer, reduced gravity model driven by observed wind stress. These authors attribute the trend in this case to the strengthening of the Walker circulation after the transition of the Pacific Decadal Oscillation from a warm to a cold equatorial phase in the last 1990s (Minobe, 2002), consistent with our results.

3.3. Interannual Variability and the Pivot Point

As noted earlier, an interesting feature of equatorial sea level variability is the presence of a "pivot" point near the center of the basin about which the modeled sea level along the equator has a tendency to tip up and down, as in a see-saw. The "pivot" point is associated with the "tilt" mode of Clarke (2010). Along the equator, the gradient of sea level associated with the "tilt" mode is close to being in equilibrium with the zonal wind stress. In the simplest example, the anomalous (departure from the mean) zonal wind stress is uniform along the equator and the corresponding anomalous (departure from the mean) sea level associated with the "tilt" mode varies linearly along the equator, with a zero crossing near the center of the basin (see Figure 2e in Zhu et al. (2017) and the discussion thereon). The sea level variability associated with the "tilt" mode therefore tips up and down, as in a see-saw, about the zero crossing; what we refer to here as the "pivot" point. In reality, most of the variability in zonal wind stress along the equator is found in the western Pacific (see Figure 2a in Zhu et al., 2017) with the result that the "pivot point" moves westward, as

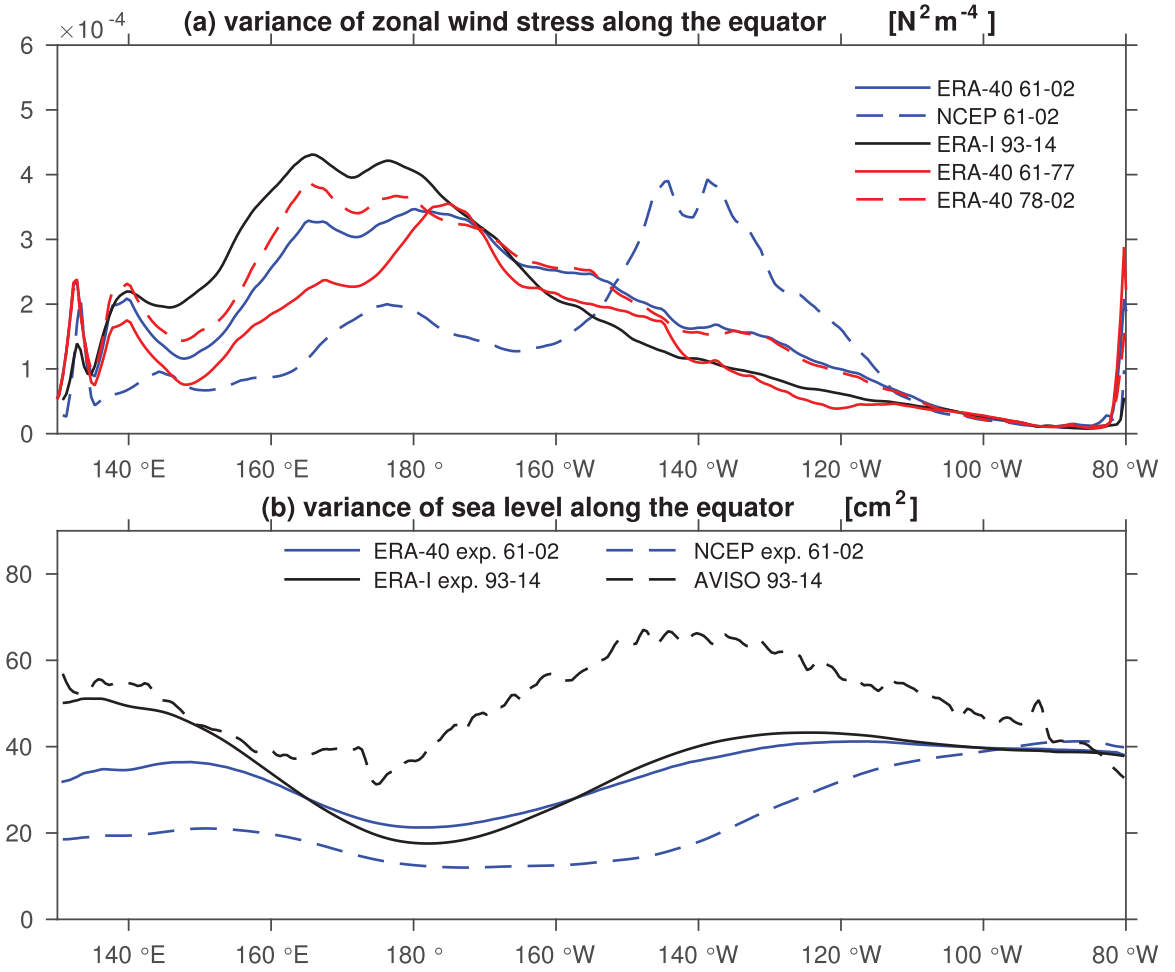

Figure 6. Variance in monthly means of (a) zonal wind stress anomalies from NCEP/NCAR, ERA-40 and ERA-Interim and (b) model-computed sea level anomalies along the equator from the NCEP/NCAR and ERA-40 experiments and the experiment in Zhu et al. (2017) driven by ERA-Interim monthly wind stress anomalies. Also shown is the variance of monthly mean sea level anomalies from AVISO.

can be seen by comparing Figures 2c and 2e in Zhu et al. (2017). It follows, as noted by Zhu et al. (2017), that the location of the pivot point is determined by the longitude range over which the zonal wind stress exhibits the largest temporal variability.

Figure 6 shows the variance of monthly zonal wind stress and sea level along the equator as a function of longitude in the different model experiments and also in AVISO. The peak in zonal wind stress variability from NCEP/NCAR near 140°W is associated with the spurious trend in this product noted in section 3.2. Apart from the peak, the variability in zonal wind stress tends to be less in the NCEP/NCAR than in the ERA-40 product and this is reflected in the lower variability in the model-computed sea level in this case shown in Figure 6b. The minimum in variance of sea surface height, reflecting the location of the pivot point, is also broader, less clearly defined and extends further to the east in the NCEP/NCAR than in the ERA-40 experiment. It is notable that all three model versions, including that discussed by Zhu et al. (2017), show generally lower variability in sea level than AVISO. This is similar to the finding of Nagura and McPhaden (2010) who compared sea level variability as seen by AVISO with sea level variability from a simple model for the Indian Ocean, a model with similarities to the one used here (see section 1). It is also notable that the minimum in sea level variance is shifted eastward in the model

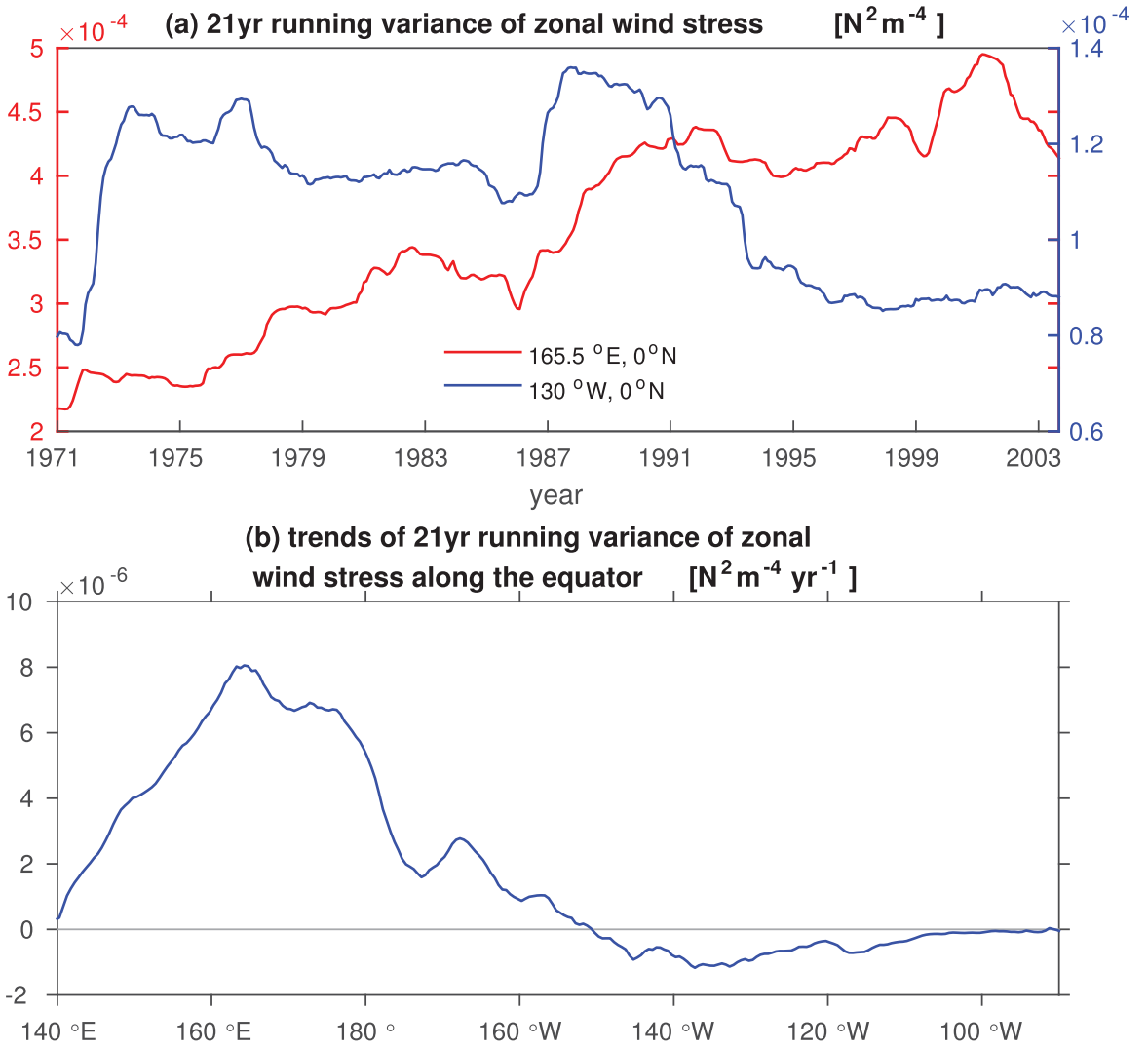

Figure 7. (a) Time series of the variance in monthly mean zonal wind stress at 165.5°E (red line) and 130°W (blue line) on the equator in 21 year running windows. (b) The trend in the time series of the variance of zonal wind stress in 21 year running windows plotted as a function of longitude along the equator and covering the time period 1961–2014. Note that the ERA-40 product is used from 1961 to 1992 and the ERA-Interim product from 1993 to 2014.

Table 1
The Percentage of Variance Explained by Each of the First Two EOFs for Sea Level Variability Along the Equator Computed From AVISO and in the Different Model Experiments (ERA-I Refers to the Standard Experiment in Zhu et al. (2017) *Covering the Period 1993–2014)*

	EOF1 (%)	EOF2 (%)	Correlation
AVISO	71	19	0.84 (0.39)
ERA-I	72	20	0.84 (0.42)
ERA-40 (61-02)	70	23	0.77 (0.30)
NCEP (61-02)	70	22	0.82 (0.30)

Note. Also shown is the correlation between the principal component time series of EOF1 and the zonal mean of the zonal wind stress along the equator (the 95% significance levels based on the method of Ebisuzaki (1997) are indicated in the brackets).

compared to AVISO. The eastward shift in the pivot point compared to AVISO was noted by Zhu et al. (2017) who attributed this error to the lack of zonal advection in the model (Dewitte et al., 2013), as noted earlier.

Also shown in Figure 6a is the variance of the zonal wind stress from ERA-40 in the subperiods 1961–1977 and 1978–2002, before and after the 1976–1977 climate shift (Trenberth et al., 1998). A notable increase and westward shift in zonal wind stress variance is found after the climate shift in the western equatorial Pacific in the ERA-40 product and there is a further increase in variance in the ERA-Interim product covering the period 1993–2014. By contrast, in the eastern tropical Pacific, the increase in zonal wind stress variance after the climate shift, i.e., for the 1978–2002 period, is not found in the ERA-Interim product covering 1993–2014. This issue is explored further in Figure 7a, where 21 year running windows are used to compute the zonal wind stress variance (the ERA-40 product is used from 1961 to 1992 and the ERA-Interim product from 1993 to 2014). The situation in the western equatorial Pacific is illustrated on the equator at 165.5°E, where there is a systematic increase in zonal wind variance throughout the study period, with no evidence of any influence from the 1976 to 1977 climate shift or, indeed, of the Pacific Decadal Oscillation which is known to have changed phase in both 1976–1977 and 1998–1999 (Minobe, 2002). Somewhat different behavior is seen further east on the equator at 130°W. Figure 7b shows the trend in zonal wind stress variance, again using 21 year running means over the period 1961–2002, but this time as a function of longitude along the equator. From this figure, one can see that the upward trend in zonal wind stress variance is found throughout the equatorial Pacific west of 160°W with very little trend in variance further east. The situation in the western equatorial Pacific is consistent with the westward shift in the region of zonal wind stress variability, especially after 1999, that has been noted by Lübbecke and McPhaden (2014). From what we show here, however, the increase in zonal wind stress variance in the western equatorial Pacific seems to be part of a much longer time scale trend than considered by these authors.

Comparing the model-computed sea level variability shown in Figure 2 for the period 1961–2002 with Figure 2 from Zhu et al. (2017) for the period 1993–2014 leaves the impression that the pivot point is located further west in the later period. This can be quantified by computing Empirical Orthogonal Functions (EOFs) from monthly mean sea level anomalies along the equator, for both the different model experiments and for AVISO. Doing this, one finds that the first EOF typically explains about 70% and the second mode around 20% of the variance, indicating their dominance (see Table 1). The spatial pattern and principal component (PC) time series associated with the first two EOFs computed from AVISO are shown in Figure 8. For AVISO, EOF1 explains 71% and EOF2 19% of the variance. The prominent El Niño events of 1997–1998 and 2009–2010 are clearly evident, especially in the PC times series for EOF1. EOF1 corresponds to what Clarke (2010) calls the "tilt" mode, for which the tilt in sea level along the equator is close to being in equilibrium with the zonal wind stress (Clarke, 2010). Indeed, the PC time series for EOF1 is highly correlated with the time series of the zonal mean of the zonal wind stress (0.84 in the case of AVISO and wind stress from ERA-Interim; see Table 1). In what follows, the longitude of the zero crossing in the spatial structure of EOF1 will be taken as the location of the pivot point.

EOF1 is shown in Figure 9a for AVISO, the two model runs, ERA-40 and NCEP/NCAR for the period 1961–2002, and the standard model run from Zhu et al. (2017) that is driven by wind stress anomalies from ERA-Interim for the period 1993–2014. It is clear that the zero crossing (and by implication the pivot point) is located further to the west in AVISO than in the model runs, consistent with the previous discussion. In the case of the NCEP/NCAR experiment, the zero crossing is located some 30° further east than in AVISO, a bias that has its origin in the spurious trend in the NCEP/NCAR wind stress product. Focusing on the more reliable ERA-40 experiment, we see a westward shift of almost 10° longitude in the zero crossing in the model experiment from Zhu et al. (2017) compared to the ERA-40 experiment discussed here. This is the shift we anticipated earlier and is a consequence of the increase and westward shift in the zonal wind stress variance along the equator in the western Pacific shown in Figures 6 and 7b.

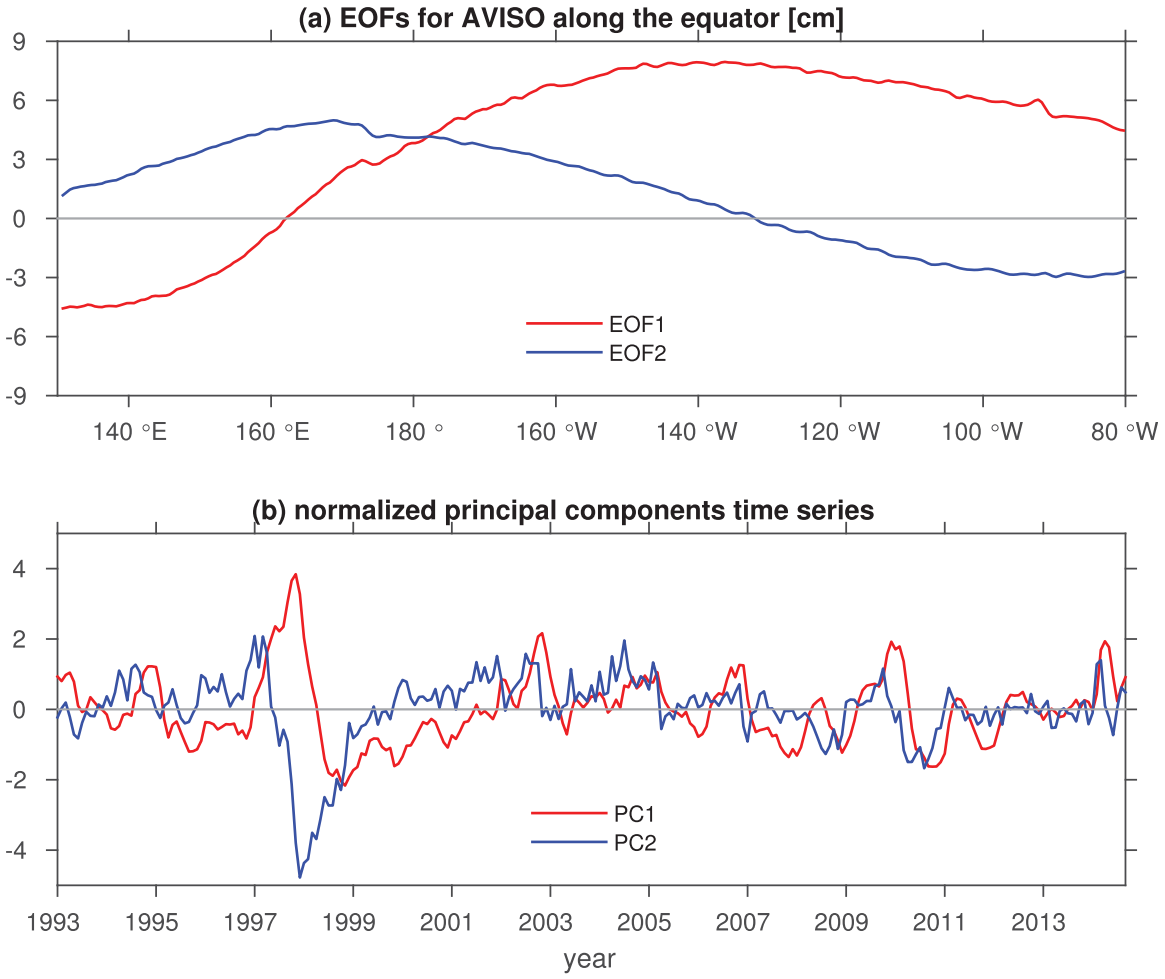

Figure 8. The (a) spatial structure and (b) principal component time series for the first two EOFs of sea level variability along the equator from AVISO (PC1: red line; PC2: blue line). The PC time series are normalized by their respective standard deviations.

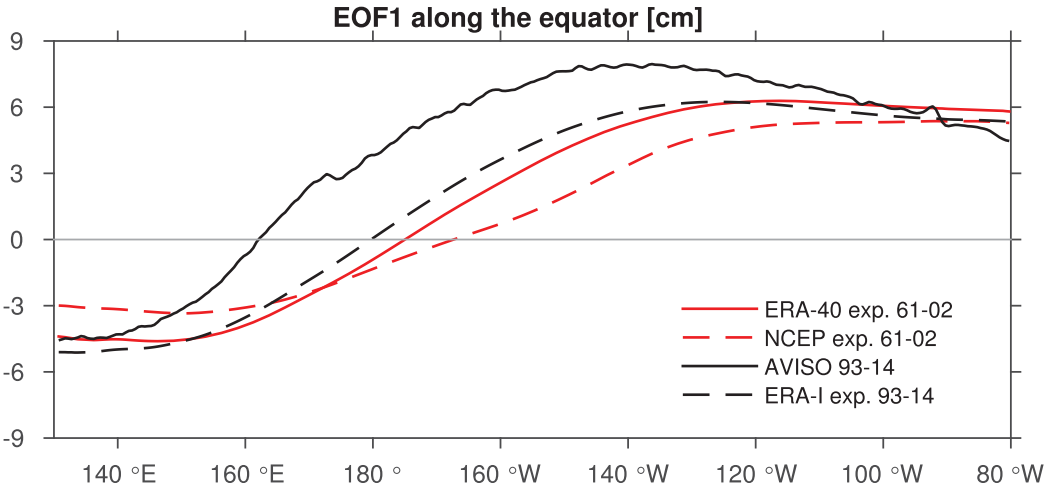

Figure 9. The first EOF of sea level variability along the equator from the full length of the model reconstructions and from AVISO.

4. Summary and Discussion

We have used the linear, multimode model of Zhu et al. (2017) to reconstruct monthly mean sea level variability in the tropical Pacific using monthly mean wind stress anomalies from the NCEP/NCAR and ERA-40 wind reanalysis. Zhu et al. (2017) noted that their model-computed sea level agrees well with the satellite-derived sea level provided by AVISO. Here the analysis period of 1961–2002 is mostly before the satellite era and includes the 1976–1977 climate shift (Trenberth et al., 1998). The simulated sea level anomalies capture the major ENSO events and generally compare well with the sea level anomalies measured by the available tide gauges shown in Figure 3, although the events in the modeled time series at Christmas Island have lower amplitude than observed. An exception is the tide gauge station at Kanton Island, which is located in the region with the lowest correlation between the model-computed sea level and AVISO (Zhu et al., 2017). The reduced correlation is due to the misplacement in the model of the pivot point along the equator associated with the "tilt" model of Clarke (2010)—see Zhu et al. (2017) for a detailed discussion.

The origin of the trend in sea level in both experiments is explored using sensitivity experiments driven by only the zonal wind stress anomalies from the NCEP/NCAR and ERA-40 products. In both cases, the spatial pattern of the sea level trend is well-captured in the sensitivity experiments compared to the experiments driven by both components of the wind stress, indicating the importance of the zonal wind stress for determining the trends in sea level in the tropical Pacific. Compared to ERA-40, NCEP/NCAR-zonal wind stress anomalies exhibit a much larger eastward trend in the eastern-central tropical Pacific that Pohlmann et al. (2017) conclude is spurious. It follows that the much larger upward trend in sea level in the eastern tropical Pacific in the NCEP/NCAR compared to the ERA-40 experiment is also, almost certainly, spurious.

We noted that the relatively poor model performance at Kanton Island is due to the presence of a pivot point along the equator about which sea level has a tendency to tip, as in a sea-saw. This behavior is the manifestation of the "tilt" mode that has been discussed by Clarke (2010) by which the tilt in sea level along the equator is close to being in equilibrium with the zonal wind stress. As noted by Zhu et al. (2017), the pivot point in the model is located to the east of the pivot point in the satellite data, i.e., AVISO, behavior that was attributed to the missing zonal advection in the model. A way to quantify the location of the pivot point is to identify its location with the zero crossing of the first EOF for sea level computed from data along the equator. The extreme eastward location of the pivot point in the experiment driven by the NCEP/NCAR wind stress product is another indication of the spurious trend in this wind stress product. The analysis also shows a more westward location in the pivot point during the period 1993–2014 than in the ERA-40 experiment. We attribute the westward shift in the pivot point to an increase and westward shift in zonal wind stress variance in the western equatorial Pacific throughout the period 1961–2002. This increase in zonal wind stress variance seems to be independent of the Pacific Decadal Oscillation and part of a much longer time scale mode of variability, possibility related to anthropogenic climate change, and requiring further study.

Acknowledgments
We thank two reviewers for their helpful comments. Xiaoting Zhu is grateful for funding from the China Scholarship Council (201306330071). This study has also been supported by the Deutsche Forschungsgemeinschaft as part of the Sonderforschungsbereich 754 "Climate-Biogeochemistry interactions in the Tropical Ocean," by the German Ministry for Education and Research (BMBF) through MiKlip2,subproject 01LP1517D (ATMOSMODINI) and SACUS (03G0837A), and by the European Union 7th Framework Programme (FP7 2007–2013) under grant agreement 603521 PREFACE project. R.J.G. is grateful to GEOMAR for continuing support. The data used in this study are available at data.geomar.de.

References

Ashok, K., Behera, S. K., Rao, S. A., Weng, H., & Yamagata, T. (2007). El Niño modoki and its possible teleconnection. *Journal of Geophysical Research*, *112*, C11007. https://doi.org/10.1029/2006JC003798

Becker, M., Meyssignac, B., Letetrel, C., Llovel, W., Cazenave, A., & Delcroix, T. (2012). Sea level variations at tropical pacific islands since 1950. *Global and Planetary Change*, *80*, 85–98.

Berrisford, P., Dee, D., Fielding, K., Fuentes, M., Kallberg, P., Kobayashi, S., et al. (2009). The ERA-interim archive. *ERA Report Series*, *1*, 1–16.

Bordbar, M. H., Martin, T., Latif, M., & Park, W. (2015). Effects of long-term variability on projections of twenty-first century dynamic sea level. *Nature Climate Change*, *5*(4), 343.

Bunge, L., & Clarke, A. J. (2014). On the warm water volume and its changing relationship with ENSO. *Journal of Physical Oceanography*, *44*(5), 1372–1385.

Busalacchi, A. J., & O'brien, J. J. (1981). Interannual variability of the equatorial Pacific in the 1960's. *Journal of Geophysical Research*, *86*(C11), 10901. https://doi.org/10.1029/JC086iC11p10901

Busalacchi, A. J., Takeuchi, K., & O'brien, J. J. (1983). Interannual variability of the equatorial Pacific Revisited. *Journal of Geophysical Research*, *88*(C12), 7551. https://doi.org/10.1029/JC088iC12p07551

Capotondi, A., Wittenberg, A. T., Newman, M., Di Lorenzo, E., Yu, J.-Y., Braconnot, P., et al. (2015). Understanding ENSO diversity. *Bulletin of the American Meteorological Society*, *96*(6), 921–938.

Church, J. A., Clark, P. U., Cazenave, A., Gregory, J. M., Jevrejeva, S., Levermann, A., et al. (2013). Sea level change. In *Climate change 2013: The physical science basis. Contribution of working group I to the fifth assessment report of the intergovernmental panel on climate change* (Technical report number 13). Cambridge, UK: Cambridge University Press.

Clarke, A. J. (2010). Analytical theory for the quasi-steady and low-frequency equatorial ocean response to wind forcing: The "tilt" and "warm water volume" modes. *Journal of Physical Oceanography*, *40*(1), 121–137.

Dewitte, B., Yeh, S.-W., & Thual, S. (2013). Reinterpreting the thermocline feedback in the western-central equatorial pacific and its relationship with the ENSO modulation. *Climate Dynamics*, *41*(3–4), 819–830.

Ebisuzaki, W. (1997). A method to estimate the statistical significance of a correlation when the data are serially correlated. *Journal of Climate*, *10*(9), 2147–2153.

Gill, A. E. (1982). *Atmosphere-ocean dynamics (International Geophysics Series)*. Cambridge, MA: Academic Press.

Holgate, S. J., Matthews, A., Woodworth, P. L., Rickards, L. J., Tamisiea, M. E., Bradshaw, E., et al. (2013). New data systems and products at the permanent service for mean sea level. *Journal of Coastal Research*, *29*(3), 493–504.

Kalnay, E., Kanamitsu, M., Kistler, R., Collins, W., Deaven, D., Gandin, L., et al. (1996). The NCEP/NCAR 40-year reanalysis project. *Bulletin of the American Meteorological Society*, *77*(3), 437–471.

Lübbecke, J. F., & McPhaden, M. J. (2014). Assessing the twenty-first-century shift in ENSO variability in terms of the Bjerknes stability index. *Journal of Climate*, *27*(7), 2577–2587.

McCreary, J. (1981). A linear stratified ocean model of the equatorial undercurrent. *Philosophical Transactions of the Royal Society of London A*, *298*(1444), 603–635.

Minobe, S. (2002). Interannual to interdecadal changes in the Bering Sea and concurrent 1998/99 changes over the north pacific. *Progress in Oceanography*, *55*(1), 45–64.

Nagura, M., & McPhaden, M. J. (2010). Dynamics of zonal current variations associated with the Indian Ocean dipole. *Journal of Geophysical Research*, *115*, C11026. https://doi.org/10.1029/2010JC006423

Pohlmann, H., Kröger, J., Greatbatch, R. J., & Müller, W. A. (2017). Initialization shock in decadal hindcasts due to errors in wind stress over the tropical pacific. *Climate Dynamics*, *49*(7), 2685–2693. https://doi.org/10.1007/s00382-016-3486-8.

PSMSL (2016). *Permanent Service for Mean Sea Level (PSMSL), "Tide gauge data"*. Retrieved from http://www.psmsl.org/data/obtaining/, accessed 23 November 2016

Qiu, B., & Chen, S. (2012). Multidecadal sea level and gyre circulation variability in the northwestern tropical pacific ocean. *Journal of Physical Oceanography*, *42*(1), 193–206.

Rhein, M., Rintoul, S., Aoki, S., Campos, E., Chambers, D., Feely, R., et al. (2013). Observations: Ocean. In *Climate change 2013: The physical science basis. Contribution of working group I to the fifth assessment report of the intergovernmental panel on climate change* (Technical report number 3). Cambridge, UK: Cambridge University Press.

Timmermann, A., McGregor, S., & Jin, F.-F. (2010). Wind effects on past and future regional sea level trends in the southern indo-pacific*. *Journal of Climate*, *23*(16), 4429–4437.

Trenberth, K. E., Branstator, G. W., Karoly, D., Kumar, A., Lau, N.-C., & Ropelewski, C. (1998). Progress during toga in understanding and modeling global teleconnections associated with tropical sea surface temperatures. *Journal of Geophysical Research*, *103*(C7), 14291–14324. https://doi.org/10.1029/97JC01444

Uppala, S. M., Kållberg, P., Simmons, A., Andrae, U., Bechtold, V., Fiorino, M., et al. (2005). The era-40 re-analysis. *Quarterly Journal of the Royal Meteorological Society*, *131*(612), 2961–3012.

Wang, C., & Fiedler, P. C. (2006). ENSO variability and the eastern tropical pacific: A review. *Progress in Oceanography*, *69*(2), 239–266.

Zhu, X., Greatbatch, R. J., & Claus, M. (2017). Interannual variability of tropical pacific sea level from 1993 to 2014. *Journal of Geophysical Research: Oceans*, *122*, 602–616. https://doi.org/10.1002/2016JC012347